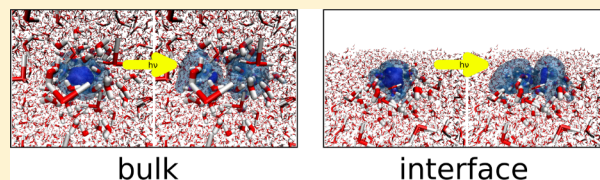


Optical Spectroscopy of the Bulk and Interfacial Hydrated Electron from Ab Initio Calculations

Frank Uhlig,[†] John M. Herbert,^{*,‡} Marc P. Coons,[‡] and Pavel Jungwirth^{*,†}[†]Institute of Organic Chemistry and Biochemistry, Academy of Sciences of the Czech Republic, Flemingovo nám. 2, CZ-16610 Prague 6, Czech Republic[‡]Department of Chemistry and Biochemistry, The Ohio State University, Columbus, Ohio 43210, United States

S Supporting Information

ABSTRACT: The optical spectrum of the hydrated (aqueous) electron, e_{aq}^- , is the primary observable by means of which this species is detected, monitored, and studied. In theoretical calculations, this spectrum has most often been simulated using one-electron models. Here, we present ab initio simulations of that spectrum in both bulk water and, for the first time, at the water/vapor interface, using density functional theory and its time-dependent variant. Our results indicate that this approach provides a reliable description, and quantitative agreement with the experimental spectrum for the bulk species is obtained using a “tuned” long-range corrected functional. The spectrum of the interfacial electron is found to be very similar to the bulk spectrum.



INTRODUCTION

Solvated electrons in ammonia and some organic solvents persist long enough for their blue color to be easily observed with the naked eye,¹ and these species were suggested as the charge carriers in solutions of alkali metals as early as 1908.² In contrast, experimental evidence for existence of a shorter-lived “hydrated electron” (e_{aq}^-) was first obtained only in 1962,³ when its optical spectrum was measured following pulsed radiolysis of liquid water. By now, the optical spectrum of e_{aq}^- is well-characterized under a variety of thermodynamic conditions^{4–6} and serves as the primary experimental observable by means of which this species is interrogated. As such, reproducing the absorption spectrum of e_{aq}^- (peaking at 1.7 eV = 720 nm under ambient conditions, with a long tail toward higher excitation energies⁶) often serves as a first test of any theoretical model of this species.

Early theoretical studies of the optical spectrum of e_{aq}^- ,^{7,8} based on one-electron quantum/classical models and electron–water pseudopotentials, concluded that the dominant feature in the spectrum arises from three heterogeneously broadened $s \rightarrow p$ transitions of a particle in a quasi-spherical (but fluctuating) solvent cavity, a conclusion that stands up to detailed, all-electron ab initio calculations.^{9–11} For a “particle in a spherical box” model that affords the experimental peak intensity and vertical ionization energy (IE), these three $s \rightarrow p$ excitations are the only dipole-allowed, bound-state transitions.¹² However, whereas atomistic one-electron models often do a reasonable job of reproducing the position and width of the main feature in the optical spectrum,^{11,13,14} in the absence of some treatment of electronic polarization of the solvent in the excited states of e_{aq}^- , such models are uniformly unable to reproduce the long, Lorentzian “blue tail” in the spectrum.^{12,14,15} More elaborate one-electron models, which introduce excited-state solvent

polarization, *do* obtain a blue tail.^{11,12} This tail, which represents higher excited states, is suggested to arise due to polarization-assisted intensity borrowing (from the dipole-allowed $s \rightarrow p$ transitions) on the part of higher-lying particle in a box states as well as “quasi-continuum” states, that is, frustrated plane waves.^{11,12}

In a recent study by one of us,¹⁶ all-electron time-dependent density functional theory (TD-DFT) calculations were used to compute the optical spectrum of e_{aq}^- within a mixed quantum/classical (QM/MM) framework. The motivation for that study was to compare TD-DFT optical spectra computed from trajectory ensembles generated by various one-electron pseudopotential models,^{13,14,17} as an effort to gauge the reliability of such models and also to comment on the recent¹⁷ and controversial^{18–20} claim that the electron might *not* localize into a cavity. Only the cavity-forming models were found to afford TD-DFT optical spectra in reasonable agreement with experiment,¹⁶ despite the fact that other observables such as the resonance Raman spectrum and the temperature dependence of the peak spectral intensity are better reproduced using the non-cavity-forming pseudopotential model.²¹

Whereas the TD-DFT calculations in ref 16 used static snapshots from one-electron pseudopotential simulations, some of us^{22,23} have recently performed QM/MM molecular dynamics simulations of both the bulk species e_{aq}^- ²² as well as the hydrated electron at the water/vapor interface,²³ with QM regions of up to 64 water molecules. The picture emerging

Special Issue: Kenneth D. Jordan Festschrift

Received: January 14, 2014

Revised: February 27, 2014

Published: February 27, 2014

from these calculations is that of a hydrated electron having a complex structure with a dominant cavity contribution but also with a significant diffuse (interstitial) part, as well as a part that overlaps the solvating water molecules.^{22,23} (It should be noted that even cavity-forming one-electron models predict significant penetration of the unpaired electron into its second solvation shell, with the water fully returning to the bulk-like structure only in the third solvation shell.^{12,14})

In the present work, the aforementioned QM/MM simulations of the bulk and interfacial hydrated electron^{22,23} are used to provide snapshots to which the TD-DFT QM/MM protocol of ref 16 can be applied. The result is a consistent *ab initio* picture of the optical spectrum of the hydrated electron. A simulation for the interfacial spectrum, for which no experiment exists yet, is presented here for the first time.

THEORETICAL METHODS

Electronic Structure Calculations. Structures investigated here are taken from simulations of a hydrated electron in bulk water²² and at the water surface.²³ The stride between the structures is 100 fs, allowing one to obtain a reasonable number of structures that are not too correlated with one another. Excitation energies are calculated using TD-DFT in its spin-unrestricted, linear response formulation.²⁴ The QM subsystem in these QM/MM calculations is $(\text{H}_2\text{O})_N^-$ ($N = 64$ for the ground-state molecular dynamics simulations), with a larger number of more distant water molecules incorporated using the simple point charge (SPC) water model.²⁵ Ground-state QM/MM molecular dynamics simulations were performed using the CP2K program,²⁶ and TD-DFT QM/MM calculations were performed using both NWChem²⁷ and Q-Chem.^{28,29}

Benchmark excited-state calculations for small QM regions were performed with $N = 4$ – 6 QM water molecules and 1020 MM water molecules. For these small systems, we performed equation-of-motion coupled cluster calculations including single and double excitations (EOM-CCSD),³⁰ for a variety of atom-centered Gaussian basis sets and compared these results to TD-DFT excitation energies obtained using different functionals. The BLYP functional^{31,32} was used as a representative of the family of generalized gradient approximations (GGAs), the hybrid B3LYP functional^{33,34} as a representative example of functionals that include Hartree–Fock exchange, and the LRC- μ BLYP³⁵ and LRC- μ BOP³⁶ functionals (see ref 37 for notation) as representative examples of long-range-corrected (LRC) functionals. In the LRC functionals, the quantity μ represents the range separation parameter, which we have ultimately “tuned” in a nonempirical way³⁸ to obtain a bulk spectrum that agrees well with the experimental result.

Excited-state properties of a four-water molecule anionic cluster embedded in a nonequilibrium polarizable continuum model³⁹ were obtained with Gaussian 09.⁴⁰ Both the B3LYP and LRC- μ BLYP functionals in combination with a 6-31++G** basis set were employed.

To evaluate the spectra of the bulk and interfacial hydrated electron, we took snapshots from the aforementioned ground-state QM/MM simulations^{22,23} for use in TD-DFT calculations. For the latter, large QM regions extending to 7.5 Å around the centroid of the ground-state spin density (which was estimated *a priori* using a one-electron pseudopotential model¹³) were selected. This results in an average of $N = 71$ QM water molecules in calculations involving the bulk species and $N = 58$ QM water molecules for the interfacial hydrated

electron, that is, values that are comparable to the $N = 64$ QM water molecules used to propagate the ground-state dynamics. Following the protocol established in ref 16, additional water molecules out to a radius of 50 Å were included as SPC point charges, employing periodic replicas of the simulation cell. For each snapshot, 15 excited states were computed at the TD-DFT/6-31++G* level within the Tamm–Dancoff approximation (TDA).⁴¹ Spectra were constructed by binning the excitation energies, weighted by oscillator strengths, into a histogram.

Results presented in the Supporting Information (SI), for a smaller QM region of 5.5 Å, show that spectra computed within the TDA are virtually identical to full TD-DFT results, despite the fact that the Thomas–Reiche–Kuhn sum rule^{42,43} is not rigorously satisfied within the TDA. Additional convergence tests reported in the SI demonstrate that reducing the QM region from 7.5 to 5.5 Å (for an average of 29 rather than 71 QM water molecules) has very little effect on the spectrum, and reducing the number of snapshots by a factor of 2 leaves the spectrum virtually unchanged. Furthermore, the LRC- μ BOP and LRC- μ BLYP functionals afford qualitatively similar spectra when the same value of μ is used for both, although the peak absorption intensity shifts by 0.2 eV. Finally, enlarging the basis set from 6-31++G* to 6-31(1+3+)⁺G*, the latter of which has been used in several previous hydrated electron studies,^{11,44,45} does not shift the intensity maximum at all and has only a minor effect on the width of the spectrum. All of these convergence tests are consistent with those reported in a previous study¹⁶ and suggest that our QM/MM TD-DFT protocol affords converged spectra, such that differences in the various spectra plotted below are primarily attributable to the choice of the functional.

Analysis. All analyses of electron and spin densities were performed on grid-based data in the Gaussian cube file format.⁴⁶ The norm and the center of the electron density are given according to standard moment analysis, and the radius of gyration (r_g) is taken as the square root of the trace of the gyration tensor.

Only excitations from the singly occupied molecular orbital (SOMO) contribute significantly to the absorption spectrum. The calculations do not suffer from any significant spin contamination; hence, the square of the SOMO essentially coincides with the spin density of the system. As such, spin densities in the excited states are reconstructed from the sum of the ground-state spin density and the density difference for the corresponding electronic excitation.

RESULTS AND DISCUSSION

The optical absorption spectrum of the hydrated electron consists of a main Gaussian feature peaked at 1.7 eV (corresponding to 720 nm) at room temperature and pressure,⁶ which is attributed to three nearly degenerate $s \rightarrow p$ excitations of a particle in a cavity^{7,8,11,15} (“spherical box” model¹²). Many more higher-lying excitations, with an overall Lorentzian line shape,⁶ are collectively referred to as the “blue tail”.

Model System. We find it useful to start the discussion with a model system for the hydrated electron. In previous work,⁴⁷ we used a small model consisting of four water molecules solvating an excess charge, with the whole $(\text{H}_2\text{O})_4^-$ model system embedded in a nonequilibrium version of the polarizable continuum model for the aqueous solvent. The first three excitation energies and oscillator strengths of this model are given in Table 1, along with the radii of gyration of the

Table 1. Excitation Energies (ω), Oscillator Strengths (f_{osc}), and Radii of Gyration (r_g) of the Excited-State Spin Densities for a Model $(\text{H}_2\text{O})_4^-/\text{PCM}$ Cluster

	ω/eV	f_{osc}	$r_g/\text{\AA}$
B3LYP ^a	1.62	0.308	4.02
	2.02	0.303	3.94
	2.02	0.303	3.94
LRC- μ BLYP ^a	1.86	0.320	3.84
	2.23	0.356	3.67
	2.23	0.356	3.67

^aWith the 6-31++G** basis set.

excited-state spin densities. Note that the model system has D_{2d} symmetry, which forces a degeneracy between the second and third excited states.

The functionals B3LYP and LRC- μ BLYP both afford comparable energetics and oscillator strengths for the low-lying excited states of this model system, which are close in energy to the main feature in the experimental spectrum at around 1.7 eV. Given the crudeness of the continuum approximation, these results support not only the utility of this model system but also the idea that although the vertical detachment energy (VDE) is subject to long-range polarization effects,^{12,14} the excitation spectrum is dominated by short-range solvent structure.¹⁶ Longer-range electronic reorganization effects, while qualitatively important,^{12,14} can be adequately described using either a relatively small QM region or (as in the present model case) a continuum solvation model.

Spin densities

$$s(\vec{r}) = \rho_\alpha(\vec{r}) - \rho_\beta(\vec{r}) \quad (1)$$

for the three excited states of this model system are shown in Figure 1. For the B3LYP calculations, the spin densities tend to be more diffuse and asymmetric than those for LRC- μ BLYP calculations, and one can also observe that parts of the electron localize more strongly on the O–H bonds pointing away from the center of the cluster in the B3LYP calculations. In any case, the p-like character of the excited states is clearly evident, which

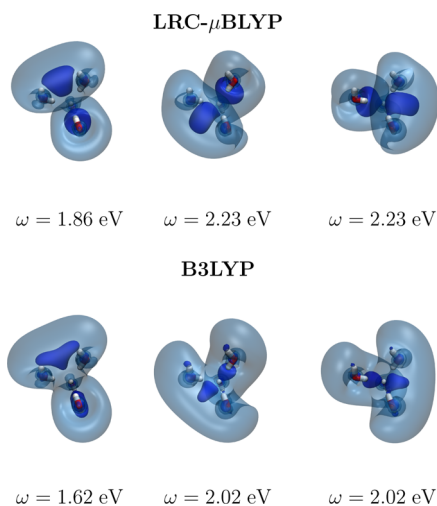


Figure 1. First three excited-state spin densities from LRC- μ BLYP/ and B3LYP/6-31++G** calculations. Shown are isosurfaces at 0.001 and 0.0001 au^{-1} , and the latter isosurface always encompasses about 85% of the spin density.

is also seen in larger QM models of the bulk hydrated electron.¹¹

A reduced description of the ground- and excited-state spin densities $s(\vec{r})$ proves to be informative. This reduced description consists of the angle-averaged radial profile $s(r)$, where $r = 0$ coincides with the centroid of $s(\vec{r})$. For the model system, the centers of the electron density in its ground and excited states are very close to each other; therefore, in Figure 2, we show only the profiles with respect to the center of the ground-state spin density. The degeneracy of the second and third excitations is reflected in identical spin density profiles for these two excitations. It is also evident from the integrated radial spin densities in Figure 2 that the B3LYP functional affords more diffuse excited-state densities, which is possibly a symptom of the residual self-interaction error (sometimes called the delocalization error⁴⁸) that is partially removed by the better asymptotic behavior of the LRC- μ BLYP exchange–correlation potential.

Benchmarking. As a first set of benchmarks for our TD-DFT calculations, we selected 60 snapshots from a trajectory of the bulk hydrated electron, representing a portion of the trajectory in which no exchange of water molecules is observed in the first solvation shell surrounding the unpaired electron. The four water molecules nearest to the electron were taken to be the QM region, and the remaining water molecules (from both the original QM region in the QM/MM simulation as well as the MM simulation cell) were described by SPC point charges.

A previous study⁴⁹ found that the peak in the main feature of the optical spectrum can be estimated using just the first three excitation energies (ω_i), weighted by their oscillator strengths (f_i)

$$E_{\text{max}} \approx \frac{\sum_{i=1}^3 \omega_i f_i}{\sum_{i=1}^3 f_i} \quad (2)$$

The location of the peak in the absorption intensity, according to this equation, is given in Table 2 for TD-DFT and EOM-CCSD calculations in various basis sets. In all of these cases, E_{max} is blue-shifted relative to the experimental spectrum, a shift that presumably originates due to significant electronic reorganization effects^{11,12,14} that cannot be captured with such a small number of QM water molecules and a static MM environment. Addition of diffuse and polarization functions lowers the excitation energies in each case, but the energetics are converged to within ± 0.05 eV already with the 6-31++G* basis set. Excitation energies calculated with BLYP are generally too low for all basis sets, which is typical behavior for GGA functionals in a noncovalent cluster environment.^{50–53} The excitation energies computed using B3LYP coincide within ± 0.01 eV with the EOM-CCSD results, whereas the LRC- μ BLYP calculations show an overestimation of about 0.2 eV. The oscillator strengths as calculated with LRC- μ BLYP/6-31++G* deviate on average by a total value of 0.02 from the EOM-CCSD reference, whereas with B3LYP, the deviation is 0.04 on average.

The range separation parameter in the LRC functionals can be tuned,³⁸ for example, to fulfill the IE condition

$$\text{IE} = -\epsilon_{\text{SOMO}} \quad (3)$$

Here, $-\epsilon_{\text{SOMO}}$ denotes the highest occupied molecular orbital eigenvalue. This tuning procedure is illustrated in Figure 3 for

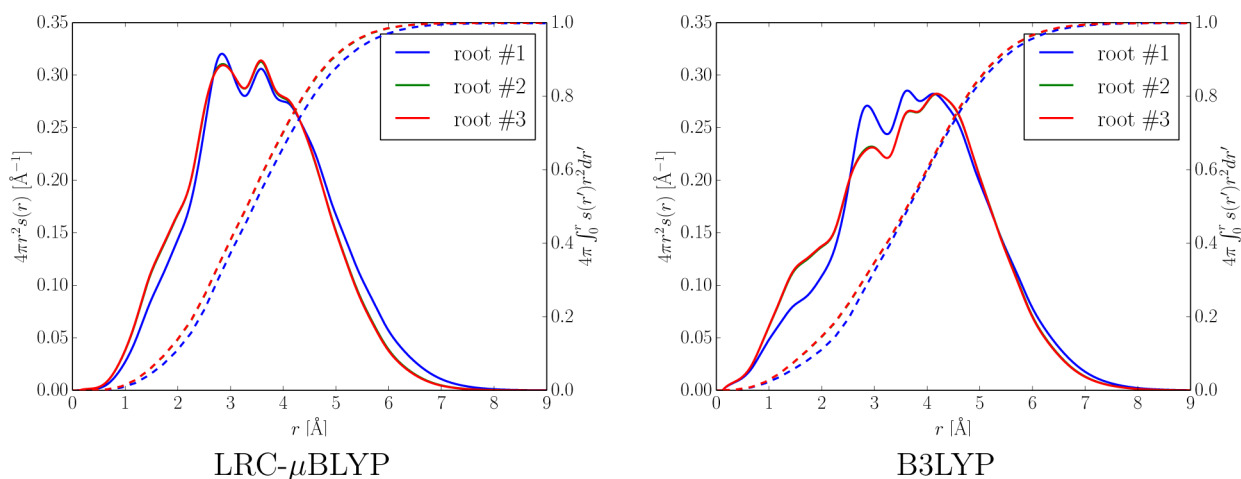


Figure 2. Radial profiles, computed using two different density functionals, of the excited-state spin densities for the lowest three excited states of an idealized $D_{2d}(\text{H}_2\text{O})_4^-$ in a polarizable continuum model of the hydrated electron. Solid curves (read from the scale at the left) denote the radial spin density profiles $4\pi r^2 s(r)$, where $r = 0$ represents the centroid of the spin density. Broken curves (read from the scale at the right) depict the cumulative radial integral of this quantity.

Table 2. Absorption Maximum (in eV) Evaluated According to Equation 2 for a Set of 60 Snapshots Each with Four QM Water Molecules

	BLYP	B3LYP	LRC- μ BLYP	EOM-CCSD
6-31G	3.29	3.54	3.92	4.61
6-31G*	3.28	3.54	3.93	4.61
6-31+G*	2.68	2.81	3.05	3.08
6-31++G*	2.20	2.28	2.49	2.26
6-31++G**	2.19	2.26	2.47	2.26
6-311++G**	2.16	2.24	2.46	2.28

the LRC- μ BOP and LRC- μ BLYP density functionals, where we plot $-e_{\text{SOMO}}$ and also the ΔSCF value of the IE

$$\text{IE}_{\Delta\text{SCF}} = E_{\text{neutral}} - E_{\text{anion}} \quad (4)$$

averaged over all 60 structures as a function of the range separation parameter, μ . According to this analysis, the optimal parameters are 0.34 a_0^{-1} for LRC- μ BLYP and 0.30 a_0^{-1} for LRC- μ BOP. These values are reasonably close to ones that, in other studies, have been statistically optimized (rather than “tuned”) by fitting small-molecule TD-DFT calculations to benchmark

data.^{36,54–56} In the case of LRC- μ BOP, for example, a statistically optimal value of $\mu = 0.33 \text{ a}_0^{-1}$ was determined,³⁶ and similarly, $\mu = 0.30 \text{ a}_0^{-1}$ was obtained for the LRC- ω PBE functional.⁵⁶ (See ref 37 for the LRC functional nomenclature.) Furthermore, a value of $\mu = 0.25 \text{ a}_0^{-1}$ for LRC- μ BOP, tuned according to eq 3, was previously determined for a $(\text{H}_2\text{O})_6^-$ cluster.¹⁶

Ultimately we apply the tuning criterion in eq 3 to the bulk e_{aq}^- spectrum; therefore, we first tested its efficacy in small-cluster benchmarks. To this end, we selected five $(\text{H}_2\text{O})_6^-$ cluster geometries with various symmetries (C_2 , C_{2v} , and D_{2h}). These structures were optimized (subject to a constraint on point group symmetry) at the MP2 level with a aug-cc-pVDZ basis set with additional diffuse functions added to all atoms. These were obtained by scaling the smallest diffuse exponents by a factor of 0.125. Range separation parameters in the LRC- μ BLYP and LRC- μ BOP functionals were tuned separately for each cluster.

Table 3 shows the average signed deviation of the TD-DFT first excited state relative to an EOM-CCSD calculation in the same basis set. For the BLYP and B3LYP methods, the deviation is reduced as the number of diffuse and polarization

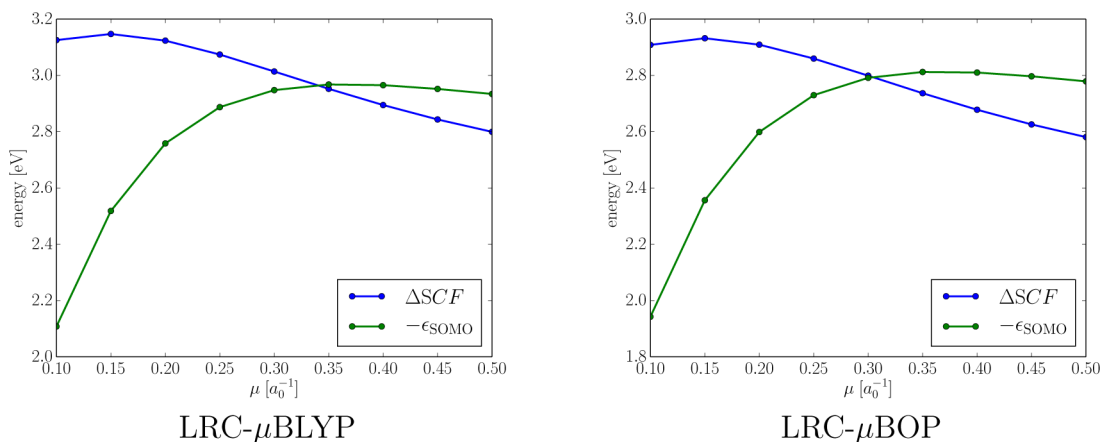


Figure 3. Tuning curves for the functionals LRC- μ BLYP and LRC- μ BOP as a function of the range separation parameter, μ . Green curves show $-\epsilon_{\text{SOMO}}$ and blue curves show the ΔSCF value of the IE (eq 4), both averaged over all 60 structures in the benchmark data set.

Table 3. Averaged Signed Deviation (relative to EOM-CCSD, in eV) of the Lowest Excitation Energies in a Set of Five $(\text{H}_2\text{O})_6^-$ Clusters

	BLYP	B3LYP	LRC- μ BLYP	LRC- μ BOP
6-31G	0.15	0.19	0.03	-0.03
6-31G*	0.16	0.17	0.02	-0.03
6-31+G*	0.15	0.12	0.01	-0.03
6-31++G*	0.14	0.11	0.06	0.01
6-31++G**	0.14	0.11	0.06	0.01
6-311++G**	0.11	0.08	0.03	-0.01

functions is increased, converging to 0.1 eV for 6-311++G**. For the tuned LRC functionals, the deviations never exceed ± 0.06 eV for any basis set that we have tested.

Condensed-Phase Spectra. We now turn our attention to the spectrum of the hydrated electron using larger QM regions and snapshots extracted from QM/MM simulations. Details of the simulation protocol were discussed in the Theoretical Methods section, and extensive convergence tests of this protocol are provided in the SI and in ref 16. Using this protocol, the position of the maximum absorption intensity appears to be converged with respect to sampling, the choice of the basis set, and the size of the QM region; hence, we can use this procedure to evaluate differences between DFT functionals. This will be our initial focus.

In previous TD-DFT studies,^{11,16} the bulk spectrum of e_{aq}^- was computed using LRC- μ BOP with $\mu = 0.37 \text{ a}_0^{-1}$, similar to the value $\mu = 0.33 \text{ a}_0^{-1}$ that was found to afford accurate VDEs for small water cluster anions.^{14,57} A tuning procedure, applied to an isomer of $(\text{H}_2\text{O})_6^-$,¹⁶ suggested a value of $\mu = 0.25 \text{ a}_0^{-1}$ instead, but in ref 16, we justified the choice $\mu = 0.37 \text{ a}_0^{-1}$, based on the fact that excitation energies varied only slightly as a function of μ , at least in the range of $\mu = 0.33\text{--}0.37 \text{ a}_0^{-1}$.^{11,16} Moreover, these larger values of μ (as compared to the “tuned” value, $\mu = 0.25 \text{ a}_0^{-1}$) afforded more accurate VDEs as compared to CCSD(T) benchmarks, although the difference is <0.1 eV.¹⁶

In the present calculations, however, we find that the value $\mu = 0.37 \text{ a}_0^{-1}$ leads to a substantially blue-shifted spectrum, as demonstrated below. On the basis of extensive testing with increasingly large QM regions in the TD-DFT calculations, it does not appear that this sizable blue shift can be eliminated by including more QM water molecules (see also the SI). Therefore, we decided to reinvestigate the tuning procedure, using some of the QM/MM snapshots that were subsequently used to simulate the spectrum.

Figure 4 illustrates the tuning procedure for three well-separated snapshots that contain 68–71 QM water molecules. The SOMO is increasingly destabilized as μ increases, which is consistent with the gradual elimination of the self-interaction error (as μ increases) that tends to overstabilize half-filled orbitals. The IE changes more slowly as a function of μ . An optimally tuned value of $\mu = 0.165 \text{ a}_0^{-1}$ is determined from the three individual tuning snapshots presented in Figure 4. This value is substantially smaller than those used in previous DFT and TD-DFT studies,^{11,14,16,57} which, however, leave a gap of ~ 0.3 eV between the Δ SCF value of the IE and $-\epsilon_{\text{SOMO}}$. This is significantly larger than the gap observed in tuning plots for $(\text{H}_2\text{O})_6^-$,¹⁶ indicating that the tuned value of μ is not transferable across substantially different system sizes. Size dependence in the optimal value of μ has been noted before in TD-DFT studies of polycyclic aromatic hydrocarbons.^{37,58}

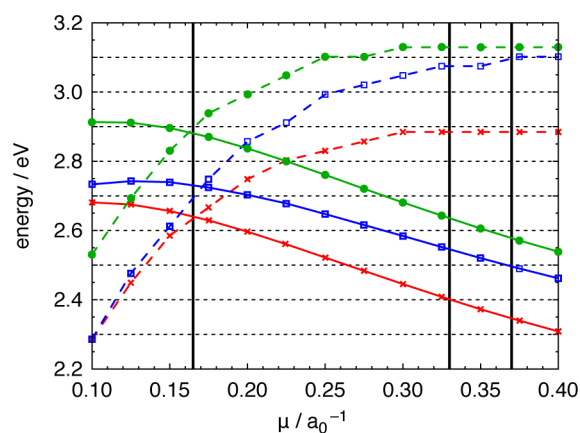


Figure 4. LRC- μ BOP/6-31++G* tuning procedure, illustrated for three different QM/MM snapshots (shown in red, green, and blue) of the bulk hydrated electron, with 68–71 QM water molecules. Solid curves depict the IE computed as a function of μ , using a Δ SCF procedure, while broken curves show the value of $-\epsilon_{\text{SOMO}}$ for the same snapshot. The optimally tuned value occurs where solid and broken curves of the same color intersect. Solid vertical lines indicate values of μ that have been used in hydrated electron studies, that is, $\mu = 0.33 \text{ a}_0^{-1}$ (ref 57), $\mu = 0.37 \text{ a}_0^{-1}$ (refs 11. and 16), and $\mu = 0.165 \text{ a}_0^{-1}$ (this work), which provides a good match to the condition $\text{IE} = -\epsilon_{\text{SOMO}}$ for all three snapshots.

Figure 5 shows the optical spectra of the bulk species computed with two versions of the LRC- μ BOP functional,

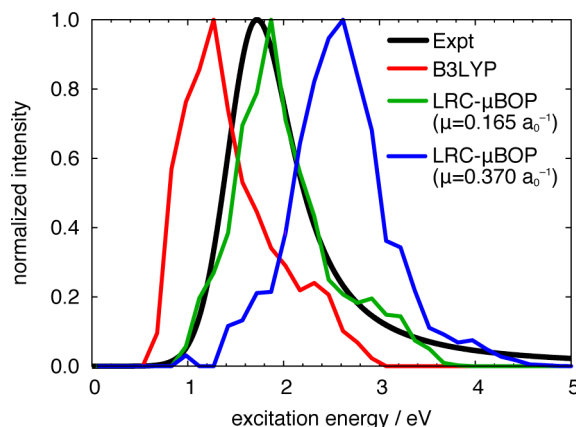


Figure 5. Absorption spectra for the bulk hydrated electron computed at the TD-DFT/6-31++G* level, using the QM/MM protocol described in the text. A total of 15 excited states (weighted by oscillator strengths and binned in 0.15 eV intervals) are included for each of 86 snapshots taken from the ground-state QM/MM simulations in 100 fs intervals. The experimental spectrum is obtained from line shape parameters reported in ref 6.

namely, one with $\mu = 0.165 \text{ a}_0^{-1}$ (tuned using the data in Figure 4) and one with $\mu = 0.370 \text{ a}_0^{-1}$ (as used in refs 11 and 16). The spectrum computed using B3LYP is also shown for comparison. Owing to the extensive convergence tests discussed above,¹⁶ we interpret the differences relative to experiment as intrinsic behavior of the functionals themselves. In particular, we observe that the B3LYP spectrum is red-shifted by about 0.4 eV. On the one hand, a B3LYP red shift is consistent with the tendency of non-LRC hybrid functionals to underestimate excitation energies for excitations in clusters and molecular liquids.^{50–53} On the other hand, however, it is eye-

opening (and rather disconcerting) to note that this shift would be difficult to infer from the small-cluster benchmarks presented in the Benchmarking subsection, where the errors (relative to EOM-CCSD calculations) in B3LYP versus LRC- μ BOP were quite comparable and offered no real reason to prefer one functional over the other.

In the bulk spectra plotted in Figure 5, the tuned LRC- μ BOP result is in a very close agreement with experiment, with the main feature in the simulated spectrum being blue-shifted by only 0.1–0.2 eV and with a width that is comparable to that of the experimental spectrum. A sizable blue tail is evident in all spectra, and the tail predicted by the tuned LRC- μ BOP functional agrees reasonably well with experiment until the intensity of the simulated spectrum (which includes only the lowest 15 excited states) dies out at around 3.5 eV. Note that basis set effects are larger for the higher-lying excited states,¹² many of which are frustrated plane waves.^{11,12}

In contrast to the above result, the spectrum computed with the larger value of μ that was used in previous work^{11,16} is blue-shifted by about 0.8 eV relative to experiment (Figure 5). The main effect responsible for this blue shift is an overstabilization of the SOMO for larger μ . (See the tuning plot in Figure 4 and note that $\epsilon_{\text{virtual}} - \epsilon_{\text{occupied}}$ is the leading term in any TD-DFT excitation energy.) A previous ab initio molecular dynamics study¹⁰ of e_{aq}^- also pointed out a systematic shift in the position (but not the shape) of the absorption spectrum as an ad hoc self-interaction correction was modified.

Given the nearly quantitative agreement between the optical spectrum computed with the tuned LRC- μ BOP functional and the experimental spectrum, one wonders whether the same value of μ can be used to accurately predict VDEs as well as excitation energies. Unfortunately, CCSD(T) benchmarks with good basis sets become prohibitively expensive for systems with more than about eight water molecules, and direct comparison with experiment is not feasible due to the extremely slow convergence of the VDE with respect to the number of QM water molecules. Even for the large QM regions employed here, the VDEs are <3 eV (see Figure 4), whereas experimental measurements of the bulk VDE are all $\gtrsim 3.4$ eV.^{59–62} For (H₂O)₆, however, both CCSD(T) and quantum Monte Carlo benchmarks are available,⁶³ and the value of μ obtained according to eq 3 engenders an error of <0.1 eV,¹⁶ which is probably comparable to the uncertainty in the benchmarks. (See Figure 11 of ref 16.)

The functionals employed and the details of the computational setup are slightly different in the present TD-DFT calculations as compared to the QM/MM simulations that were used to propagate the ground-state dynamics whence the snapshots were obtained.²² In particular, the trajectories were obtained using the BLYP functional in conjunction with a semiempirical self-interaction correction,^{64,65} whereas the self-interaction should be less pronounced for the hybrid and LRC functionals used in the TD-DFT calculations presented here. Given these differences, it bears noting that the radii of gyration from both the B3LYP and LRC- μ BLYP calculations presented herein compare well with the radii of gyration obtained in the original QM/MM ground-state molecular dynamics simulations.²² The mean absolute deviation in r_g as compared to the value obtained in those simulations, is only about 0.1 Å for LRC- μ BLYP and 0.2 Å for B3LYP.

That said, notable differences exist between the excited-state spin densities computed with B3LYP and LRC- μ BOP. Using an analysis scheme developed in ref 22, we can compute how

much of the excited-state spin densities reside inside of the solvent cavity occupied by the ground-state electron (Table 4),

Table 4. Average Partitioning (in %) of the First Three Excited-State Spin Densities^a

	B3LYP	LRC- μ BOP
in cavity	3	6
on water	27	31
as diffuse ^b	29	44
beyond QM/MM interface	41	19

^aOnly QM waters are considered. See ref 22 for details. ^bPortion in the interstitial spaces outside of the cavity.

and we note that the main part of the spin density in the excited state is located beyond the first solvent shell. For the B3LYP calculations, only about 60% of the excited-state spin densities are contained within the QM subsystem, while the number raises to around 80% in the case of LRC- μ BOP. The effect of this artifact on the energetics of the excited states must be relatively minor, given that the excitation energies for these states are essentially converged even in much smaller QM regions. This effect can also be visualized in the form of radial profiles of the excited-state spin density with respect to the center of the ground-state spin density, plots of which are shown in the SI.

In previous work,¹⁶ we used a similar TD-DFT/MM protocol to simulate the spectrum of e_{aq}^- along trajectories determined from various one-electron pseudopotential models.^{13,14,17} The goal was to make a direct comparison between different structural models for e_{aq}^- using the optical absorption spectrum as a figure of merit. Considering only trajectories from a polarizable one-electron model,¹⁴ with snapshots the same as those used in ref 16 but extending the QM region out to 7.5 Å for consistency with the other spectra simulated here, the corresponding TD-LRC- μ BOP/6-31++G* spectrum is plotted in Figure 6. As reported in ref 16, the spectrum using $\mu = 0.37$ a₀⁻¹ is blue-shifted by about 0.5 eV, but here, we discover that the tuned LRC- μ BOP/6-31++G* spectrum is red-shifted by about 0.3 eV. Figure 6 also shows these two spectra shifted by the respective amounts (−0.5 and +0.3 eV) necessary to get the peak position right. Following this shift, we

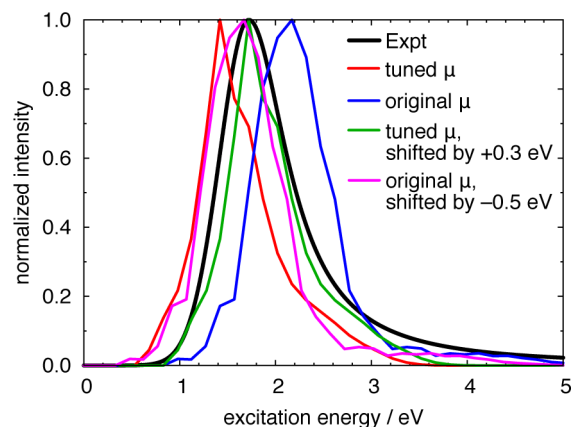


Figure 6. TD-LRC- μ BOP/6-31++G* optical spectra computed using geometries obtained from the polarizable one-electron pseudopotential model of ref 14. The figure compares results obtained using the “original” value $\mu = 0.370$ a₀⁻¹ that was used in refs 11 and 16 versus the “tuned” value $\mu = 0.165$ a₀⁻¹ used in this work.

see that the width of the main Gaussian feature is approximately correct.

As noted in previous *ab initio*⁶⁶ and one-electron pseudopotential studies,⁴⁹ excitation and ionization energies are strongly correlated to the radius of gyration of the ground-state spin density. Figure 7 plots the first three excitation

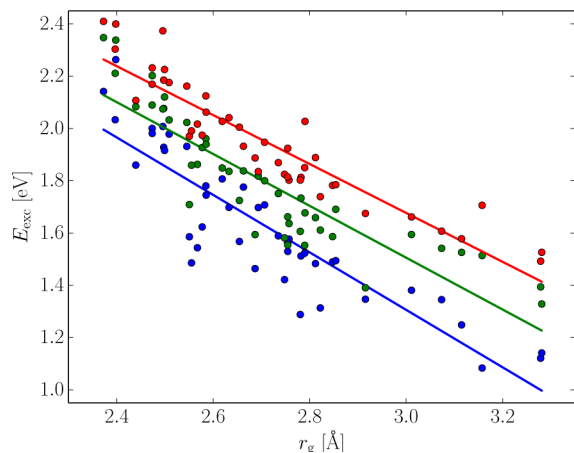


Figure 7. Correlation between the three lowest excitation energies (as computed with the tuned LRC- μ BOP/6-31++G* setup) versus the radius of gyration of the ground-state spin density. Linear regression fits to the data are shown as solid lines.

energies for the tuned LRC- μ BOP functional versus r_g for a set of snapshots. The excitation shifts to lower energies as r_g increases. This behavior is qualitatively explained (and, in the presence of more data, can be quantitatively fit to) a particle in a cavity model.⁴⁹ This analytic result suggests that the excitation energy should vary as r_g^{-2} ,⁴⁹ whereas the linear fits shown in Figure 7 each have correlation coefficients ≥ 0.9 . The pseudolinear behavior is likely a consequence of the narrow range of r_g that is sampled in the bulk hydrated electron, as compared to finite-size water cluster anions.⁴⁹ Similar behavior was observed in ref 49 comparing cluster and bulk data.

Finally, we consider an electron solvated at the water surface, that is, at the water/vapor interface. Ground-state QM/MM simulations were reported in ref 23, and the corresponding snapshots were used to compute a TD-DFT spectrum using the same protocol as that for the bulk species. A QM radius of 7.5 Å results in fewer QM water molecules, on average, as compared to the bulk snapshots. Thus, given the potential sensitivity of the tuned μ value to system size, we repeated the tuning procedure illustrated in Figure 4 using three snapshots from the interfacial simulations. This exercise results in a tuned value of $\mu = 0.180 \text{ a}_0^{-1}$ that is rather close to the value of $\mu = 0.165 \text{ a}_0^{-1}$ used to compute the spectrum of the bulk species.

The computed interfacial spectrum is shown in Figure 8 together with the bulk spectrum from Figure 5, and the two spectra are found to be close to each other. This is in accord with our previous observation that the structure of the electron solvated at the water/vapor interface is very similar to that in the aqueous bulk.²³ QM/MM simulations of electron solvation at the interface suggest that indeed its wave function does not extend significantly into vacuum,²³ which has also been inferred from surface-sensitive spectroscopic investigations of this species.⁶⁷

In previous studies of water cluster anions⁴⁹ using a one-electron pseudopotential model,¹⁴ it was noted that a high

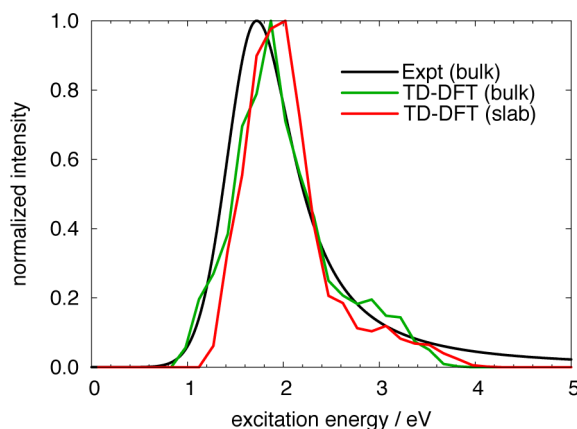


Figure 8. Absorption spectra computed for the interfacial hydrated electron at the TD-LRC- μ BOP/6-31++G* level, using the QM/MM protocol described in the text, and compared to the bulk spectrum computed with the same protocol. The value of μ was tuned separately for the bulk calculations ($\mu = 0.165 \text{ a}_0^{-1}$; see Figure 4) and the interfacial calculation ($\mu = 0.180 \text{ a}_0^{-1}$).

degree of correlation exists between r_g and the location of the electronic absorption maximum. This correlation is also borne out in QM/MM studies of photoionization (see Figure 7 and ref 66). Noting that a “partially embedded” surface isomer described in ref 49, which may be the cluster analogue of the electron at the water/vapor interface, had a radius of gyration very similar to that of the bulk species, it was predicted in ref 49 that the interfacial electron’s absorption spectrum might not differ significantly from that of the bulk species. The simulated spectra presented in Figure 8 are consistent with this prediction.

The similarity in the optical spectra of the interfacial and bulk hydrated electron can also be inferred from the radial profiles of the excited-state spin densities plotted as averaged profiles of the first three excited states in Figure 9. The first three excited

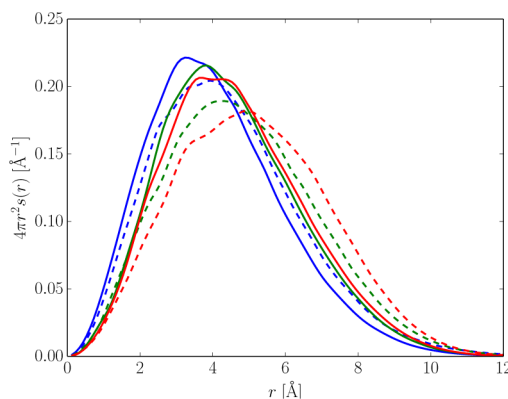


Figure 9. Radial profiles of excited-state spin densities for the first three excited states of an interfacial (solid lines) and bulk hydrated (dashed lines) electron.

states show similar radial dependence in both cases, and the peak structure is mainly due to overlap with water, as can be seen from the individually dissected radial profiles shown in the SI. The fourth and fifth excited states are more diffuse than the first three excited states. The decomposition according to ref 23 is similar for all excited states. One can note a slight decrease of about 5% in the amount of excited-state spin density that

protrudes into the vapor phase for the fourth and fifth excited states, which is redistributed over water molecules and interstitial/diffuse parts (see also the SI). This hints to one reason for the similarity of the spectra of the bulk and interface hydrated electron as it is not preferential to form weakly hydrated electrons on top of the surface but rather to overlap with water molecules in the bulk or the topmost surface layers.

CONCLUSIONS

In the present ab initio study of the hydrated electron, we have focused on evaluation of its electronic absorption spectrum. We have shown previously that the DFT description of the hydrated electron affords a complex structure of the bulk hydrated species e_{aq}^- , with a dominant cavity contribution but also a significant diffuse part and part overlapping with water molecules. TD-DFT calculations on top of these ground-state QM/MM trajectories yield a spectrum that agrees well with the experimental result, with the agreement being quantitative when tuned LRC functionals are employed. The optical spectrum of the hydrated electron at the water/vapor interface is computed here for the first time and has been found to be almost identical to that in the aqueous bulk, as anticipated in previous theoretical studies.^{23,49}

ASSOCIATED CONTENT

Supporting Information

Additional spectral calculations, additional radial profiles of the excited states, dissection of excited-state spin densities of the interfacially solvated electron into individual contributions, and averaged distances of the centers of ground- and excited- state spin densities. This material is available free of charge via the Internet at <http://pubs.acs.org>.

AUTHOR INFORMATION

Corresponding Authors

*E-mail: herbert@chemistry.ohio-state.edu.

*E-mail: pavel.jungwirth@uochb.cas.cz.

Notes

The authors declare no competing financial interest.

ACKNOWLEDGMENTS

J.M.H. and M.P.C. acknowledge financial support from the U.S. National Science Foundation (Grant No. CHE-0748448) and computing resources from the Ohio Supercomputer Center (Project No. PAA-0003). P.J. acknowledges the Czech Science Foundation (Grant P208/12/G016) for support and thanks the Academy of Sciences for the Praemium Academie award.

REFERENCES

- (1) Edwards, P. P. The Electronic Properties of Metal Solutions in Liquid Ammonia and Related Solvents. *Adv. Inorg. Chem. Radiochem.* **1982**, *25*, 135–185.
- (2) Kraus, C. A. Solutions of Metals in Non-Metallic Solvents; IV. Material Effects Accompanying the Passage of an Electrical Current through Solutions of Metals in Liquid Ammonia. Migration Experiments. *J. Am. Chem. Soc.* **1908**, *30*, 1323–1344.
- (3) Hart, E. J.; Boag, J. W. Absorption Spectrum of the Hydrated Electron in Water and in Aqueous Solutions. *J. Am. Chem. Soc.* **1962**, *84*, 4090–4095.
- (4) Jou, F.-Y.; Freeman, G. R. Shapes of Optical Spectra of Solvated Electrons. Effect of Pressure. *J. Phys. Chem.* **1977**, *81*, 909–915.

- (5) Tuttle, T. R., Jr.; Golden, S. Shape Stability of Solvated-Electron Optical Absorption Bands. Part 1.-Experimental Basis. *J. Chem. Soc., Faraday Trans. 2* **1981**, *77*, 873–888.

- (6) Coe, J. V.; Williams, S. M.; Bowen, K. H. Photoelectron Spectra of Hydrated Electron Clusters vs. Cluster Size. *Int. Rev. Phys. Chem.* **2008**, *27*, 27–51.

- (7) Rossky, P. J.; Schnitker, J. The Hydrated Electron: Quantum Simulation of Structure, Spectroscopy, and Dynamics. *J. Phys. Chem.* **1988**, *92*, 4277–4285.

- (8) Wallqvist, A.; Martyna, G.; Berne, B. J. Behavior of the Hydrated Electron at Different Temperatures: Structure and Absorption Spectrum. *J. Phys. Chem.* **1988**, *92*, 1721–1730.

- (9) Boero, M.; Parrinello, M.; Terakura, K.; Ikeshoji, T.; Liew, C. C. First-Principles Molecular-Dynamics Simulations of a Hydrated Electron in Normal and Supercritical Water. *Phys. Rev. Lett.* **2003**, *90*, 226403/1–226403/4.

- (10) Boero, M. Excess Electron in Water at Different Thermodynamic Conditions. *J. Phys. Chem. A* **2007**, *111*, 12248–12256.

- (11) Jacobson, L. D.; Herbert, J. M. Polarization-Bound Quasi-Continuum States Are Responsible for the ‘Blue Tail’ in the Optical Absorption Spectrum of the Aqueous Electron. *J. Am. Chem. Soc.* **2010**, *132*, 10000–10002.

- (12) Herbert, J. M.; Jacobson, L. D. Nature’s Most Squishy Ion: The Important Role of Solvent Polarization in the Description of the Hydrated Electron. *Int. Rev. Phys. Chem.* **2011**, *30*, 1–48.

- (13) Turi, L.; Borgis, D. Analytical Investigations of an Electron–Water Molecule Pseudopotential. II. Development of a New Pair Potential and Molecular Dynamics Simulations. *J. Chem. Phys.* **2002**, *117*, 6186–6195.

- (14) Jacobson, L. D.; Herbert, J. M. A One-Electron Model for the Aqueous Electron That Includes Many-Body Electron-Water Polarization: Bulk Equilibrium Structure, Vertical Electron Binding Energy, and Optical Absorption Spectrum. *J. Chem. Phys.* **2010**, *133*, 154106/1–154106/19.

- (15) Turi, L.; Hantal, G.; Rossky, P. J.; Borgis, D. Nuclear Quantum Effects in Electronically Adiabatic Quantum Time Correlation Functions: Application to the Absorption Spectrum of a Hydrated Electron. *J. Chem. Phys.* **2009**, *131* (), 024119/1–024119/9.

- (16) Herbert, J. M.; Jacobson, L. D. Structure of the Aqueous Electron: Assessment of One-Electron Pseudopotential Models in Comparison to Experimental Data and Time-Dependent Density Functional Theory. *J. Phys. Chem. A* **2011**, *115*, 14470–14483.

- (17) Larsen, R. E.; Glover, W. J.; Schwartz, B. J. Does the Hydrated Electron Occupy a Cavity? *Science* **2010**, *329*, 65–69.

- (18) Turi, L.; Madarász, A. Comment on “Does the Hydrated Electron Occupy a Cavity?”. *Science* **2011**, *331*, 1387.

- (19) Jacobson, L. D.; Herbert, J. M. Comment on “Does the Hydrated Electron Occupy a Cavity?”. *Science* **2011**, *331*, 1387.

- (20) Larsen, R. E.; Glover, W. J.; Schwartz, B. J. Response to Comment on “Does the Hydrated Electron Occupy a Cavity?”. *Science* **2011**, *331*, 1387.

- (21) Casey, J. R.; Larsen, R. E.; Schwartz, B. J. Resonance Raman and Temperature-Dependent Electronic Absorption Spectra of Cavity and Noncavity Models of the Hydrated Electron. *Proc. Natl. Acad. Sci. U.S.A.* **2013**, *110*, 2712–2717.

- (22) Uhlig, F.; Marsalek, O.; Jungwirth, P. Unraveling the Complex Nature of the Hydrated Electron. *J. Phys. Chem. Lett.* **2012**, *3*, 3071–3075.

- (23) Uhlig, F.; Marsalek, O.; Jungwirth, P. Electron at the Surface of Water: Dehydrated or Not? *J. Phys. Chem. Lett.* **2013**, *4*, 338–343.

- (24) Casida, M. E. In *Recent Advances in Density Functional Methods, Part I*; Chong, D. P., Ed.; Recent Advances in Computational Chemistry; World Scientific: River Edge, NJ, 1995; Vol. I, Chapter 5, pp 155–192.

- (25) Berendsen, H. J. C.; Postma, J. P. M.; van Gunsteren, W. F.; Hermans, J. *Intermolecular Forces*; Reidel: Holland, 1981; p 331.

- (26) VandeVondele, J.; Krack, M.; Mohamed, F.; Parrinello, M.; Chassaing, T.; Hutter, J. Quickstep: Fast and Accurate Density

Functional Calculations Using a Mixed Gaussian and Plane Waves Approach. *Comput. Phys. Commun.* **2005**, *167*, 103–128.

(27) Valiev, M.; Bylaska, E. J.; Govind, N.; Kowalski, K.; Straatsma, T. P.; van Dam, H. J. J.; Wang, D.; Nieplocha, J.; Apra, E.; Windus, T. L.; et al. NWChem: A Comprehensive and Scalable Open-Source Solution for Large Scale Molecular Simulations. *Comput. Phys. Commun.* **2010**, *181*, 1477–1489.

(28) Shao, Y.; Fusti-Molnar, L.; Jung, Y.; Kussmann, J.; Ochsenfeld, C.; Brown, S. T.; Gilbert, A. T. B.; Slipchenko, L. V.; Levchenko, S. V.; O'Neill, D. P.; et al. Advances in Methods and Algorithms in a Modern Quantum Chemistry Program Package. *Phys. Chem. Chem. Phys.* **2006**, *8*, 3172–3191.

(29) Krylov, A. I.; Gill, P. M. W. Q-Chem: An Engine for Innovation. *WIREs Comput. Mol. Sci.* **2013**, *3*, 317–326.

(30) Stanton, J. F.; Bartlett, R. J. The Equation of Motion Coupled-Cluster Method. A Systematic Biorthogonal Approach to Molecular Excitation Energies, Transition Probabilities, And Excited State Properties. *J. Chem. Phys.* **1993**, *98*, 7029–7039.

(31) Becke, A. D. Density-Functional Exchange-Energy Approximation with Correct Asymptotic Behavior. *Phys. Rev. A* **1988**, *38*, 3098–3100.

(32) Lee, C.; Yang, W.; Parr, R. G. Development of the Colle–Salvetti Correlation-Energy Formula into a Functional of the Electron Density. *Phys. Rev. B* **1988**, *37*, 785–789.

(33) Becke, A. D. Density-Functional Thermochemistry. III. The Role of Exact Exchange. *J. Chem. Phys.* **1993**, *98*, 5648–5652.

(34) Stephens, P. J.; Devlin, F. J.; Chabalowski, C. F.; Frisch, M. J. Ab Initio Calculation of Vibrational Absorption and Circular Dichroism Spectra Using Density Functional Force Fields. *J. Phys. Chem.* **1994**, *98*, 11623–11627.

(35) Iikura, H.; Tsuneda, T.; Yanai, T.; Hirao, K. A Long-Range Correction Scheme for Generalized-Gradient-Approximation Exchange Functionals. *J. Chem. Phys.* **2001**, *115*, 3540–3544.

(36) Tawada, Y.; Tsuneda, T.; Yanagisawa, S.; Yanai, T.; Hirao, K. A Long-Range Corrected Time-Dependent Density Functional Theory. *J. Chem. Phys.* **2004**, *120*, 8425–8433.

(37) Richard, R. M.; Herbert, J. M. Time-Dependent Density-Functional Description of the 1L_a State in Polycyclic Aromatic Hydrocarbons: Charge-Transfer Character in Disguise? *J. Chem. Theory Comput.* **2011**, *7*, 1296–1306.

(38) Baer, R.; Livshits, E.; Salzner, U. Tuned Range-Separated Hybrids in Density Functional Theory. *Annu. Rev. Phys. Chem.* **2010**, *61*, 85–109.

(39) Cossi, M.; Rega, N.; Scalmani, G.; Barone, V. Energies, Structures, And Electronic Properties of Molecules in Solution with the C-PCM Solvation Model. *J. Comput. Chem.* **2003**, *24*, 669–681.

(40) Frisch, M. J.; Trucks, G. W.; Schlegel, H. B.; Scuseria, G. E.; Robb, M. A.; Cheeseman, J. R.; Scalmani, G.; Barone, V.; Mennucci, B.; Petersson, G. A.; Nakatsuji, H.; Caricato, M.; Li, X.; Hratchian, H. P.; Izmaylov, A. F.; et al. *Gaussian 09*, revision A.1. Gaussian Inc.: Wallingford, CT, 2009.

(41) Hirata, S.; Head-Gordon, M. Time-Dependent Density Functional Theory within the Tamm–Dancoff Approximation. *Chem. Phys. Lett.* **1999**, *314*, 291–299.

(42) Fano, U.; Cooper, J. W. Spectral Distribution of Atomic Oscillator Strengths. *Rev. Mod. Phys.* **1968**, *40*, 441–507.

(43) McHale, J. L. *Molecular Spectroscopy*; Prentice Hall: Upper Saddle River, NJ, 1999.

(44) Herbert, J. M.; Head-Gordon, M. Calculation of Electron Detachment Energies for Water Cluster Anions: An Appraisal of Electronic Structure Methods, With Application to $(\text{H}_2\text{O})_{20}^-$ and $(\text{H}_2\text{O})_{24}^-$. *J. Phys. Chem. A* **2005**, *109*, 5217–5229.

(45) Herbert, J. M.; Head-Gordon, M. Accuracy and Limitations of Second-Order Many-Body Perturbation Theory for Predicting Vertical Detachment Energies of Solvated-Electron Clusters. *Phys. Chem. Chem. Phys.* **2006**, *8*, 68–78.

(46) Herbert, J. M. *Reviews in Computational Chemistry*; Wiley-VCH: New York, 2014.

(47) Uhlig, F.; Jungwirth, P. Embedded Cluster Models for Reactivity of the Hydrated Electron. *Z. Phys. Chem.* **2013**, *227*, 1583–1593.

(48) Cohen, A. J.; Mori-Sanchez, P.; Yang, W. Challenges for Density Functional Theory. *Chem. Rev.* **2012**, *112*, 289–320.

(49) Jacobson, L. D.; Herbert, J. M. Theoretical Characterization of Four Distinct Isomer Types in Hydrated-Electron Clusters, And Proposed Assignments for Photoelectron Spectra of Water Cluster Anions. *J. Am. Chem. Soc.* **2011**, *133*, 19889–19899.

(50) Bernasconi, L.; Sprik, M.; Hutter, J. Time Dependent Density Functional Theory Study of Charge-Transfer and Intramolecular Electronic Excitations in Acetone–Water Systems. *J. Chem. Phys.* **2003**, *119*, 12417–12431.

(51) Bernasconi, L.; Sprik, M.; Hutter, J. Hartree–Fock Exchange in Time Dependent Density Functional Theory: Application to Charge Transfer Excitations in Solvated Molecular Systems. *Chem. Phys. Lett.* **2004**, *394*, 141–146.

(52) Neugebauer, J.; Louwse, M. J.; Baerends, E. J.; Wesolowski, T. A. The Merits of the Frozen-Density Embedding Scheme to Model Solvatochromatic Shifts. *J. Chem. Phys.* **2005**, *122*, 094115/1–094115/13.

(53) Lange, A.; Herbert, J. M. Simple Methods to Reduce Charge-Transfer Contamination in Time-Dependent Density-Functional Calculations of Clusters and Liquids. *J. Chem. Theory Comput.* **2007**, *3*, 1680–1690.

(54) Rohrdanz, M. A.; Herbert, J. M. Simultaneous Benchmarking of Ground- And Excited-State Properties with Long-Range-Corrected Density Functional theory. *J. Chem. Phys.* **2008**, *129*, 034107/1–034107/9.

(55) Rohrdanz, M. A.; Martins, K. M.; Herbert, J. M. A Long-Range-Corrected Density Functional That Performs Well for Both Ground-State Properties and Time-Dependent Density Functional Theory Excitation Energies, Including Charge-Transfer Excited States. *J. Chem. Phys.* **2009**, *130*, 054112/1–054112/8.

(56) Lange, A. W.; Herbert, J. M. Both Intra- And Interstrand Charge-Transfer Excited States in B-DNA are Present at Energies Comparable to, or Just Above, the $^1\pi\pi^*$ Excitonic Bright States. *J. Am. Chem. Soc.* **2009**, *131*, 3913–3922.

(57) Yagi, K.; Okano, Y.; Sato, T.; Kawashima, Y.; Tsuneda, T.; Hirao, K. Water Cluster Anions Studied by Long-Range Corrected Density Functional Theory. *J. Phys. Chem. A* **2008**, *112*, 9845–9853.

(58) Wong, B. M.; Hsieh, T. H. Optoelectronic and Excitonic Properties of Oligoacenes: Substantial Improvements from Range-Separated Time-Dependent Density Functional Theory. *J. Chem. Theory Comput.* **2010**, *6*, 3704–3712.

(59) Tang, Y.; Shen, H.; Sekiguchi, K.; Kurahashi, N.; Mizuno, T.; Suzuki, Y. I.; Suzuki, T. *Phys. Chem. Chem. Phys.* **2010**, *12*, 3653–3655.

(60) Siefermann, K. R.; Liu, Y.; Lugovoy, E.; Link, O.; Faubel, M.; Buck, U.; Winter, B.; Abel, B. *Nat. Chem.* **2010**, *2*, 274–279.

(61) Shreve, A. T.; Yen, T. A.; Neumark, D. M. *Chem. Phys. Lett.* **2010**, *493*, 216–219.

(62) Lübcke, A.; Buchner, F.; Heine, N.; Hertel, I. V.; Schultz, T. *Phys. Chem. Chem. Phys.* **2010**, *12*, 14629–14634.

(63) Xu, J.; Jordan, K. D. Application of the Diffusion Monte Carlo Method to the Binding of Excess Electrons to Water Clusters. *J. Phys. Chem. A* **2010**, *114*, 1364–1366.

(64) d’Avezac, M.; Calandra, M.; Mauri, F. Density Functional Theory Description of Hole-Trapping in SiO₂: A Self-Interaction-Corrected Approach. *Phys. Rev. B* **2005**, *71*, 205210/1–205210/5.

(65) VandeVondele, J.; Sprik, M. A Molecular Dynamics Study of the Hydroxyl Radical in Solution Applying Self-Interaction-Corrected Density Functional Methods. *Phys. Chem. Chem. Phys.* **2005**, *7*, 1363–1367.

(66) Marsalek, O.; Uhlig, F.; VandeVondele, J.; Jungwirth, P. Structure, Dynamics, and Reactivity of Hydrated Electrons by Ab Initio Molecular Dynamics. *Acc. Chem. Res.* **2012**, *45*, 23–32.

(67) Sagar, D. M.; Bain, C. D.; Verlet, J. R. R. Hydrated Electrons at the Water/Air Interface. *J. Am. Chem. Soc.* **2010**, *132*, 6917–6919.